Arctic organic aerosol measurements show particles from mixed combustion in spring haze and from frost flowers in winter

P. M. Shaw,[1] L. M. Russell,[1] A. Jefferson,[2] P. K. Quinn,[3]

[1]Scripps Institution of Oceanography, University of California San Diego, La Jolla, California, USA.

[2]Cooperative Institute for Research in Environmental Science, University of Colorado Boulder, Colorado, USA

[3]Pacific Marine Environmental Laboratory, National Oceanic and Atmospheric Administration, Seattle, Washington, USA

Submicron atmospheric aerosol particles were collected between 1 March 2008 and 1 March 2009 at Barrow, Alaska, to characterize the organic mass (OM) in the Arctic aerosol. Organic functional group concentrations and trace metals were measured with FTIR on submicron particles collected on Teflon filters. The OM varied from 0.07 μg m^{-3} in summer to 0.43 μg m^{-3} in winter, and 0.35 μg m^{-3} in spring, showing a transition in OM composition between spring and winter. Most of the OM in spring could be attributed to anthropogenic sources, consisting primarily of alkane and carboxylic acid functional groups and correlated to elemental tracers of industrial pollution, biomass burning, and shipping emissions. PMF analysis associated OM with two factors, a Mixed Combustion factor (MCF) and an Ocean-derived factor (ODF). Back trajectory analysis revealed that the highest fractions of the MCF were associated with air masses that had originated from northeastern Asia and the shipping lanes south of the Bering Straits. The ODF consisted of organic hydroxyl groups and correlated with organic and inorganic seawater components. The ODF accounted for more than 55% of OM in winter when the sampled air masses originated along the coastal and lake regions of the Northwest Territories of Canada. Frost flowers with organic-salt coatings that arise by brine rejection during sea ice formation may account for this large source of carbohydrate-like OM during the ice-covered winter season. While the anthropogenic sources contributed more than 0.3 μg m^{-3} of the springtime haze OM, ocean-derived particles provided comparable OM sources in winter.

1. Introduction

Changing snow and sea ice cover, associated albedo feedbacks and large seasonal variation in incoming sunlight make the Arctic region especially sensitive to recent climate change [*Garrett et al.*, 2009]. *Li and Winchester* [1990] proposed organic carbon was a significant fraction of the total submicron aerosol mass that they measured at Barrow, and subsequent studies showed this fraction could account for 20-30% of the submicron aerosol mass concentration [*Li and Winchester*, 1993]. *Quinn et al.* [2002] measured three years of ionic species at Barrow and attributed much of the residual in the submicron mass balance to the organic components. Transported Arctic aerosol particles could result in either positive or negative feedbacks to global warming [*Tomasi et al.*, 2007], making understanding the role of organics in the Arctic atmosphere crucial for quantifying the direct and indirect aerosol effects in this sensitive region.

Long term observations of seasonal patterns in organic carbon concentration and speciation were reported by *Kawamura et al.* [1996] for Alert, Canada, and *Ricard et al.* [2002] in Sevettijarvi, Finland. In this work, we report the first year-long study of organic mass (OM) functional group composition in submicron particles in the Arctic region. The measurements were performed at the National Oceanic and Atmospheric Administration (NOAA) Earth System Research Laboratory (ESRL) site at Barrow, collocated with ongoing measurements of inorganic ions, optical, and physical metrics of aerosol particles and other atmospheric characteristics. We show that the submicron organic functional group composition provides important insight on the sources and composition of both the

well known springtime Arctic haze and the substantial OM contributions from frost flower particles in wintertime organic mass concentrations.

2. Methods

Beginning in March 2008, automated measurements were maintained by NOAA ESRL staff at their laboratory in Barrow, Alaska, using an 8-sample rotating filter holder (described by *Quinn et al.* [2002]) modified to replace materials that outgas volatile organic compounds with metal or Delrin components. The filter holder exposes 8 different 47 mm diameter Teflon filters in series to ambient air pulled through a warmed inlet at 30 L min^{-1}. Filters were exposed for 24 to 96 hr, with the 24-hr duration used in winter and spring and the 96-hr duration used during the summer when aerosol concentrations are low. Filters were sealed and frozen during transport and storage until analysis. To avoid contamination of the air from the town of Barrow, sector control was used to collect samples only when the wind speed was above 0.5 m s^{-1}, and direction was between 0°and 130°. Fourier transform infrared (FTIR) spectra were collected for each filter in a temperature and humidity controlled clean room to measure the absorption of organic functional groups and convert to mass [*Maria et al.*, 2002, 2003; *Maria and Russell*, 2005; *Gilardoni et al.*, 2007] using an automated algorithm [*Liu et al.*, 2009; *Russell et al.*, 2009a] and normalized by the recorded volume to obtain concentrations. We quantified saturated aliphatic CCH (the alkane functional group), carboxylic COH with associated C=O in an acid group COOH (the carboxylic acid functional group), non-acidic hydroxyl COH (the alcohol functional group), and primary amine CNH_2 functional groups [*Russell et al.*, 2009b]. Non-acidic carbonyl C=O, aromatic and unsaturated aliphatic (alkene) functional

groups are omitted because they were below detection limits for the majority of the study. Of the 118 filters scanned by FTIR, 47 were sent to Chester laboratories for X-ray fluorescence (XRF) spectroscopy [*Maria et al.*, 2002] to quantify S, Na, Cl, Si, Al, Fe, Ti, Ca, Mg, K, V, Zn, and Br (additional measured elements were below detection limit for a majority of samples). Ion chromatography was used to quantify ionic composition of 66 filters overlapping with the OM measurements [*Quinn et al.*, 2002].

3. Results

OM concentrations varied significantly from March 2008 to March 2009, as shown in Fig. 1. Based on OM concentration and functional group composition, we have separated the measurements into three seasons, which are summarized in Fig.1: spring (March to June), summer (July to October), and winter (November to February). These seasons were determined according to the following criteria: (1) spring months had daily-averaged OM concentrations higher than 1 μg m^{-3} and consisted of approximately half alkane groups with the other half split between carboxylic acid and alcohol functional groups in approximately equal parts; (2) summer months generally had 4-day averaged OM concentrations below 0.5 μg m^{-3} and consisted of about half alkane and half alcohol functional group fractions; (3) winter month filters generally had the highest OM concentrations and were primarily alcohol groups. A three-year aerosol study at Barrow by *Quinn et al.* [2002] used slightly different cutoffs for 1997 - 2000 to study consistent differences in the inorganic aerosol concentration and composition, with February omitted as transitional and October identified as winter. In any given year the characteristics of February and October are arguably transitional, but for OM October 2008 resembles the lower OM concentrations

and wind speeds of summer rather than those of winter (Fig. 1a). Similarly February 2009 represented a continuation of the high organic hydroxyl composition of winter rather than the carboxylic acid fraction that characterized the rest of spring.

Positive matrix factorization (PMF) provides a tool to apportion sources based on the repeated occurrence of similar spectral features during a series of ambient measurements in a single region [*Paatero and Tapper*, 1994]. PMF of FTIR spectra has been used to identify combinations of organic functional groups that combine linearly in time to reproduce the original observed OM time series [*Russell et al.*, 2009a; *Liu et al.*, 2009]. PMF was performed on the 118 spectra collected at Barrow. FPEAK rotation values of -0.2, 0, and 0.2 were tested on solutions of 2 through 6 factors resulting in negligible differences, so FPEAK = 0 is used here. We also eliminated solutions that reproduced less than 98% of the original OM concentrations. The time series of the best 2-factor solution is shown in Fig. 1b, with the associated spectra and organic functional group composition in Fig. 2a. The first PMF factor (defined as Mixed Combustion MCF) accounts for much of the carboxylic acid and alkane group concentrations, and the second factor (defined as Ocean-derived ODF) accounts for most of the organic hydroxyl group concentrations .

Correlations of tracers with the two resulting PMF factor OM concentrations are summarized in Fig. 2b for XRF metals and Fig. 2c for IC sea salt ions, and were used to identify the possible sources associated with each OM factor. We describe correlations as strong for $r>0.75$ and mild for correlations with $0.5<r<0.75$. Using these criteria, the first PMF factor is correlated strongly to S and non-dust K and mildly to V. Since V is a tracer for oil combustion (including from shipping) and non-dust K is a tracer for biomass

burning, we refer to this factor as the MCF [*Cachier et al.*, 1995; *Gilardoni et al.*, 2009; *Isakson et al.*, 2001]. The alkane and carboxylic acid group contributions to the OM are characteristic of processed emissions from oil burning and have also been seen in biomass burning [*Russell et al.*, 2009a]. The second factor correlates mildly for all IC measurements of Na^+ and Cl^-. We call this factor ODF based on this correlation to NaCl as well as the similarity of the spectrum of the second factor to other ocean-derived organic particles [*Russell et al.*, 2010].

To provide an indication of the geographic location of the emissions, potential source contribution functions (PSCF,*Pekney et al.* [2006]) were calculated from five-day (Fig. 3a,b) HYSPLIT isentropic back trajectories [*Draxler and Rolph*, 2003]. The HYSPLIT model was run every four hours during each filter with a starting altitude of 500 m. Maps of PSCF were used to indicate likely source regions of the highest 75th percentile of observations of a given factor normalized by total OM. The PSCF map for the MCF (Fig 3a) shows potential source regions over Siberia (between 60-70°N and west of 180°), which correspond with locations of forest fires observations by MODIS during the observation period (Fig. 3c). *Paris et al.* [2009] observed smoke from Siberian wildfires in the Arctic in early July. Commercial shipping traffic (Fig. 3c) was estimated from the total March 2008 to March 2009 frequency of meteorological observations reported from ships [*Corbett et al.*, 1999] and were found to overlap the high MCF PSCF regions south of 60°N between 160°and -160°. These high MCF regions also overlap industrial regions of northern Russia (surrounding Anadyr, Russia; Fig. 3c), where smelters, coal mining and other industry contribute significant anthropogenic particle emissions [*AMAP*, 1998].

4. Discussion

Long-range transported pollution from lower latitudes including black carbon, sulfates, soil dust, and biomass burning smoke have dramatic influences on what should otherwise be a clean Arctic environment [*Barrie and Barrie*, 1990]. Emissions from burning forests have been shown to produce non-acidic carbonyl groups in addition to carboxylic acid groups [*Russell et al.*, 2009a; *Liu et al.*, 2009]. The lack of non-acidic carbonyl groups in the MCF may result from the longer processing time associated with transport of these emissions from Asia as well as the contributions from other emission sources. This MCF also correlates with industrial trace metals (Fe, Zn, and Br), as shown in Fig. 2b, indicating that urban areas such as Anadyr also contributed to the MCF.

Russell et al. [2010] show that the organic hydroxyl (alcohol) functional group measured by FTIR is representative of carbohydrate-like compounds, including saccharides, associated with ocean-derived particles emitted by bubble bursting during wave breaking. The ODF at Barrow has very similar features in the FTIR spectrum (Fig. 2a), including the broad organic hydroxyl absorbance between 3200 and 3500 cm^{-1}. Because local wind speed may be a poor representation of sea salt emission in regions removed from the receptor, we averaged gridded 1°x 1°NCEP reanalysis surface winds along each five day back trajectory that passed through the boundary layer for each filter. The linear fit of trajectory weighted mean wind speed (Fig. 2d) for summer ODF compares well with the observations of a similar marine factor versus wind speed in the Arctic during ice free conditions [*Russell et al.*, 2010]. The winter best fit line has a higher dependence of particle concentration on wind speed, which is likely associated with the higher particle

production rate as a function of wind speed from frost flowers than from bubble bursting. There appears to be little OM at low wind speeds, and no OM at wind speeds above approximately 8 m s^{-1}, consistent with ranges found in other frost flower studies [*Obbard et al.*, 2009].

The potential source region identified for the ODF (Fig. 3b) overlaps in summer with the ocean and in winter with sea-ice-land fringes and the Great Bear and Great Slave lakes (Fig. 3b). The replacement of coastal waters by sea ice in winter, as well as the higher slope of the emitted ODF with average trajectory wind speed, support a different mechanism for the formation of ocean-derived organic particles in winter. These results suggest that surface frost flowers formed on the sea and lake ice provide the source of the ODF at Barrow in winter. Frost flowers grow as ice skeletons from supersaturated water vapor at the ice-air interface. Brine rejected to pools on the sea ice surface during ice formation from seawater provides a highly saline source that can be wicked up onto frost flowers [*Alvarez-Aviles et al.*, 2008] and likely includes sea water dissolved organic matter (DOM) [*Thomas and Dieckmann*, 2003; *Stein and MacDonald*, 2004; *Papadimitriou et al.*, 2007; *Giannelli et al.*, 2001; *Belzile et al.*, 2002].

The high PSCF region for the ODF factor was east of Barrow amid the islands of the Northwest Territories of Canada and is also the location of young coastal ice rivers and lakes that are ideal for frost flower formation [*Beaudon and Moore*, 2009]. To identify areas of potential frost flower (PFF) coverage, we used the same 1-d algorithm on gridded NCEP reanalysis surface temperature and sea ice concentrations as described in *Kaleschke et al.* [2004]. High density PFF regions along the northern coast of Alaska and Canada

and among the lakes of the Northwest Territories (Fig. 3d) coincide with high density of back trajectories for the ODF PSCF regions. Separating the observations with trajectories that passed over the Great Bear and Great Slave lakes from those that passed only over ocean results in stronger correlations of ODF with Na^+ and Cl^-. The ratio of NaCl to OM is about a factor of two lower for lake-influenced samples, consistent with the lower NaCl in the lakes relative to the oceans.

5. Conclusion

Twelve months of submicron particle measurements at Barrow, Alaska, show that organic components contribute significant quantities of particle mass, some of which may be light absorbing. Overall OM concentrations range from less than 0.5 μg m^{-3} in summer to often more 2 μg m^{-3} in winter and spring. Functional group composition also changed by season: alkane and carboxylic acid functional groups dominated spring composition and organic hydroxyl groups dominated winter. High OM concentrations from Asian biomass burning, ship traffic, and other industrial activities produced Arctic haze in spring, low concentrations in summer occurred when removal by precipitation is most efficient, and large concentrations in winter were caused by ocean-derived OM that is possibly released from frost flowers. Through PSCF of PMF-based OM factors, we identified the probable locations of the two types of source emissions: 1) mixed combustion from urban areas in Siberia and the shipping lanes of the North Pacific in springtime; and 2) ocean-derived particles released from bubble bursting in summer and from ocean and lake frost flowers in winter. Frost flowers provide a source of particles in the Arctic region during winter, which results in surprisingly large concentrations of Arctic OM comparable to those ob-

196 served during the springtime haze. Improved monitoring of aerosol exchange between the
197 atmosphere and surface cryosphere should be considered.

198 **Acknowledgments.** This study was funded by the National Science Foundation (NSF
199 ARC-0714052) for the International Polar Year. NCEP Daily Global Analyses data pro-
200 vided by the NOAA/OAR/ESRL PSD, Boulder, Colorado, USA, from their Web site at
201 http://www.esrl.noaa.gov/psd/. Fire images were obtained from the NASA NEESPI Data
202 and Services Center (http://gdata1.sci.gsfc.nasa.gov/). We would like to thank Kristen
203 Schulz, Lelia Hawkins, John Ogren, Pat Sheridan, Betsy Andrews, Jason Johns and the
204 staff of the NOAA ESRL Barrow station for assistance in the collection of measurements.

References

205 Alvarez-Aviles, L., W. R. Simpson, T. A. Douglas, M. Sturm, D. Perovich, and F. Domine
206 (2008), Frost flower chemical composition during growth and its implications for aerosol
207 production and bromine activation, *J. Geophys. Res.*, *113*(D21).

208 AMAP (1998), *Assessment report: Arctic pollution issues*, Arctic Monitoring and Assess-
209 ment Programme.

210 Barrie, L., and M. Barrie (1990), Chemical components of lower tropospheric aerosols in
211 the high Arctic: Six years of observations, *J. of Atmos. Chem.*, *11*(3), 211–226.

212 Beaudon, E., and J. Moore (2009), Frost flower chemical signature in winter snow on
213 Vestfonna ice cap, Nordaustlandet, Svalbard, *The Cryosphere*, *3*, 147–154.

214 Belzile, C., J. Gibson, and W. Vincent (2002), Colored dissolved organic matter and dis-
215 solved organic carbon exclusion from lake ice: Implications for irradiance transmission

and carbon cycling, *Limnology and Oceanography*, *47*(5), 1283–1293.

Cachier, H., C. Liousse, P. Buat-Menard, and A. Gaudichet (1995), Particulate content of savanna fire emissions, *Journal of Atmospheric Chemistry*, *22*(1), 123–148.

Corbett, J., P. Fischbeck, and S. Pandis (1999), Global nitrogen and sulfur inventories for oceangoing ships, *J. Geophys. Res.*, *104*(D3).

Draxler, R., and G. Rolph (2003), HYSPLIT (HYbrid Single-Particle Lagrangian Integrated Trajectory) Model access via NOAA ARL READY Website (http://www. arl. noaa. gov/ready/hysplit4. html). NOAA Air Resources Laboratory, Silver Spring.

Garrett, T. J., M. M. Maestas, S. K. Krueger, and C. T. Schmidt (2009), Acceleration by aerosol of a radiative-thermodynamic cloud feedback influencing arctic surface warming, *Geophys. Res. Letters*, *36*.

Giannelli, V., D. Thomas, C. Haas, G. Kattner, H. Kennedy, and G. Dieckmann (2001), Behaviour of dissolved organic matter and inorganic nutrients during experimental sea-ice formation, *Annals of Glaciology*, *33*(1), 317–321.

Gilardoni, S., et al. (2007), Regional variation of organic functional groups in aerosol particles on four US east coast platforms during the International Consortium for Atmospheric Research on Transport and Transformation 2004 campaign, *J. Geophys. Res*, *112*.

Gilardoni, S., et al. (2009), Characterization of organic ambient aerosol during MIRAGE 2006 on three platforms, *Atmos. Chem. Phys*, *9*, 5417–5432.

Isakson, J., T. Persson, and E. Selin Lindgren (2001), Identification and assessment of ship emissions and their effects in the harbour of Goteborg, Sweden, *Atmo. Envi.*, *35*(21),

3659–3666.

Kaleschke, L., et al. (2004), Frost flowers on sea ice as a source of sea salt and their influence on tropospheric halogen chemistry, *Geophys. Res. Lett*, *31*, L16,114.

Kawamura, K., H. Kasukabe, and L. A. Barrie (1996), Source and reaction pathways of dicarboxylic acids, ketoacids and dicarbonyls in arctic aerosols: One year of observations, *Atmo. Envi.*, *30*(10-11), 1709–1722.

Li, S. M., and J. W. Winchester (1990), Haze and other Aerosol omponents in late winter Arctic Alaska, 1986, *J. Geophys. Res.*, *95*(D2), 1797–1810.

Li, S. M., and J. W. Winchester (1993), Water-soluble organic-constituents in Arctic aerosols and snow pack, *Geophys. Res. Let.*, *20*(1), 45–48.

Liu, S., S. Takahama, L. Russell, S. Gilardoni, and D. Baumgardner (2009), Oxygenated organic functional groups and their sources in single and submicron organic particles in MILAGRO 2006 campaign, *Atmos. Chem. Phys. Discuss*, *9*, 4567–4607.

Maria, S., and L. Russell (2005), Organic and inorganic aerosol below-cloud scavenging by suburban New Jersey precipitation, *Environ. Sci. Technol*, *39*(13), 4793–4800.

Maria, S., L. Russell, B. Turpin, and R. Porcja (2002), FTIR measurements of functional groups and organic mass in aerosol samples over the Caribbean, *Atmo. Envi.*, *36*(33), 5185–5196.

Maria, S., L. Russell, B. Turpin, R. Porcja, T. Campos, R. Weber, and B. Huebert (2003), Source signatures of carbon monoxide and organic functional groups in Asian Pacific Regional Aerosol Characterization Experiment (ACE-Asia) submicron aerosol types, *J. Geophys. Res*, *108*, 8637.

Obbard, R., H. Roscoe, E. Wolff, and H. Atkinson (2009), Frost flower surface area and chemistry as a function of salinity and temperature, *J. Geophys. Res.*, *114*(D20), D20,305.

Paatero, P., and U. Tapper (1994), Positive matrix factorization: A non-negative factor model with optimal utilization of error estimates of data values, *Environmetrics*, *5*(2), 111–126.

Papadimitriou, S., D. Thomas, H. Kennedy, C. Haas, H. Kuosa, A. Krell, and G. Dieckmann (2007), Biogeochemical composition of natural sea ice brines from the Weddell Sea during early austral summer, *Limnology and Oceanography*, *52*(5), 1809–1823.

Paris, J., A. Stohl, P. Nédélec, M. Arshinov, M. Panchenko, V. Shmargunov, K. Law, B. Belan, and P. Ciais (2009), Wildfire smoke in the Siberian Arctic in summer: source characterization and plume evolution from airborne measurements, *Atmos. Chem. & Phys. Discussions*, *9*, 18,201–18,233.

Pekney, N., C. Davidson, L. Zhou, and P. Hopke (2006), Application of PSCF and CPF to PMF-Modeled Sources of PM 2.5 in Pittsburgh, *Aerosol Science and Technology*, *40*(10), 952–961.

Quinn, P. K., T. L. Miller, T. S. Bates, J. A. Ogren, E. Andrews, and G. E. Shaw (2002), A 3-year record of simultaneously measured aerosol chemical and optical properties at Barrow, Alaska, *J. Geophys. Res.*, *107*(D11).

Ricard, V., J. Jaffrezo, V. Kerminen, R. Hillamo, M. Sillanpaa, S. Ruellan, C. Liousse, and H. Cachier (2002), Two years of continuous aerosol measurements in northern Finland, *J.Geophys. Res.*, *107*(D11), 4129.

Russell, L., S. Takahama, S. Liu, L. Hawkins, D. Covert, P. Quinn, and T. Bates (2009a), Oxygenated fraction and mass of organic aerosol from direct emission and atmospheric processing measured on the R/V Ronald Brown during TEXAQS/GoMACCS 2006, *J. Geophys. Res*, *114*.

Russell, L., R. Bahadur, L. Hawkins, J. Allan, D. Baumgardner, P. Quinn, and T. Bates (2009b), Organic aerosol characterization by complementary measurements of chemical bonds and molecular fragments, *Atmos. Envi.*

Russell, L., L. Hawkins, A. Frossard, P. Quinn, and T. Bates (2010), Carbohydrate-like composition of submicron atmospheric particles and their production from ocean bubble bursting, *Proc. National Academy of Sciences*.

Stein, R., and R. MacDonald (2004), *The organic carbon cycle in the Arctic Ocean*, Springer Verlag.

Thomas, D., and G. Dieckmann (2003), *Sea ice: an introduction to its physics, chemistry, biology and geology*, Blackwell Publishing.

Tomasi, C., et al. (2007), Aerosols in polar regions: A historical overview based on optical depth and in situ observations, *J. Geophys. Res.*, *112*(D16).

1 Figure 1

Time series of measured atmospheric aerosol component concentrations. a) FTIR organic functional groups; b) PMF factors; c) XRF trace metals; d) IC sea salt. Bar widths correspond to durations of collected filters. Inset pies indicate time weighted seasonal averages.

2 Figure 2

Results of two-factor PMF solution. a) Baselined spectra. Colors for spectra correspond to those given in Fig. 1b. Inset pies indicate the fractional functional group composition for each factor; b) correlations of MCF and XRF trace metal concentrations (S: r=0.96; non-dust K: r=0.80; V: r=0.61; Fe: r=0.69; Zn: r=0.69; Br: r=0.68); c) correlations of ODF and IC salt concentrations (overall Cl^-: r=0.63; Na^+: r=0.60), with separate lines for filters influenced by lakes (solid lines; Cl^-: r=0.86; Na^+: r=0.77) and ocean-only (dashed lines; Cl^-: r=0.74; Na^+: r=0.81); d) back trajectory-weighted mean wind speed versus ODF observations with fraction >0.5 for summer (red; [ODF]=0.037∗wind speed - 0.17; r=0.87) and winter (blue; [ODF]=0.24∗wind speed - 0.84; r= 0.67).

3 Figure 3

Density maps of a) 5-day PSCF for MCF (highest in dark orange); b) 5-day PSCF for ODF (highest in dark blue); c) anthropogenic sources: cities with population >10000 (Anadyr, Russia; Barrow, Fairbanks, Anchorage and Juneau, Alaska); estimated shipping density from NCEP marine observations for observation period (highest in dark red); MODIS fire locations for observation period (greyscale); d) modeled density of potential frost flower regions for observation period (highest in dark purple).

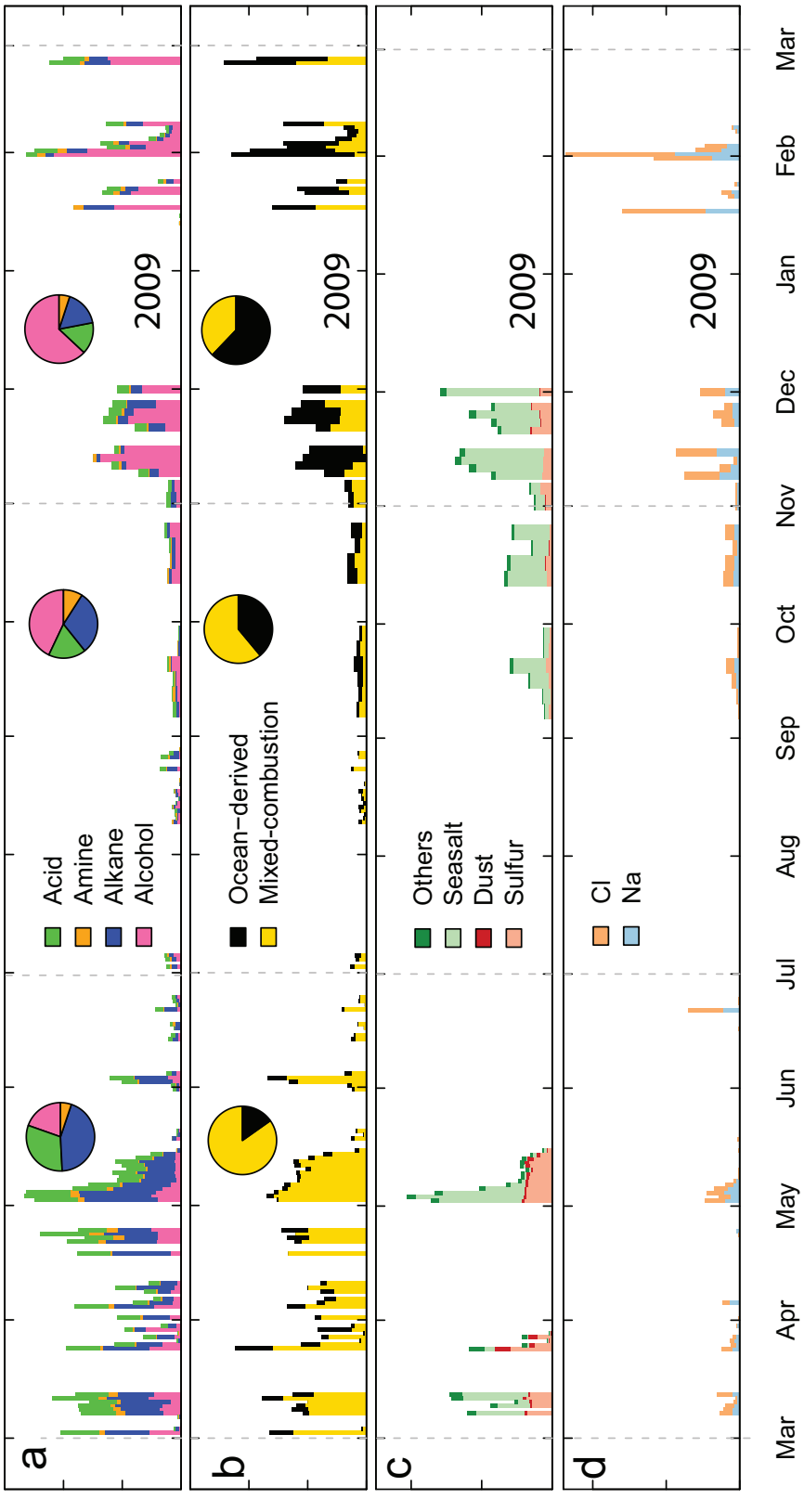
a
b
c
d
2009
Acid
Amine
Alkane
Alcohol
Ocean−derived
Mixed−combustion
Others
Seasalt
Dust
Sulfur
Cl
Na
concentration (μg m⁻³)
Mar
Apr
May
Jun
Jul
Aug
Sep
Oct
Nov
Dec
Jan
Feb
Mar

Figure 1:

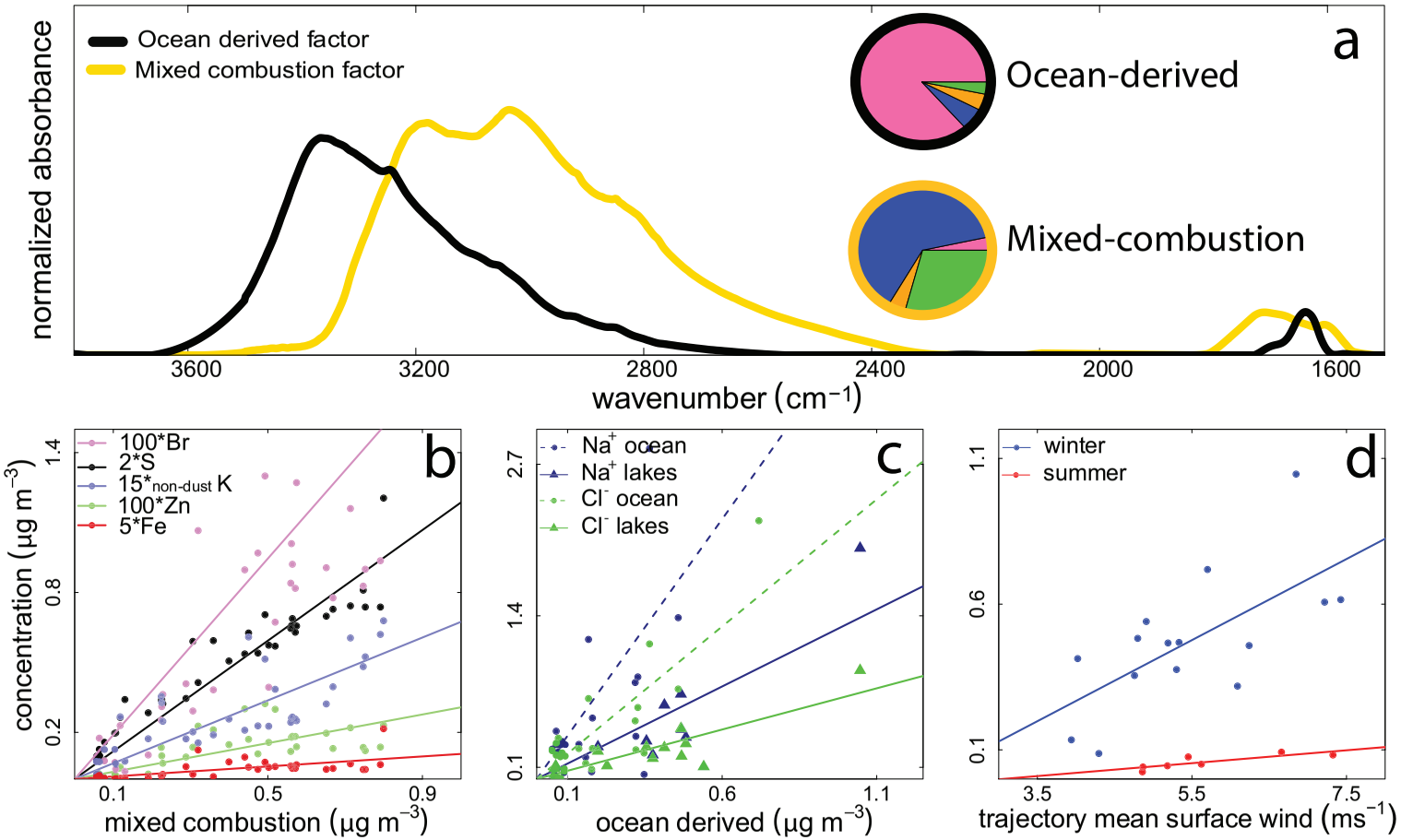
a
Ocean derived factor
Mixed combustion factor
normalized absorbance
Ocean-derived
Mixed-combustion
3600
3200
2800
2400
2000
1600
wavenumber (cm^{-1})
b
100*Br
2*S
15*non-dust K
100*Zn
5*Fe
concentration (µg m^{-3})
0.2
0.8
1.4
0.1
0.5
0.9
mixed combustion (µg m^{-3})
c
Na$^+$ ocean
Na$^+$ lakes
Cl$^-$ ocean
Cl$^-$ lakes
0.1
1.4
2.7
0.1
0.6
1.1
ocean derived (µg m^{-3})
d
winter
summer
0.1
0.6
1.1
3.5
5.5
7.5
trajectory mean surface wind (ms^{-1})

Figure 2:

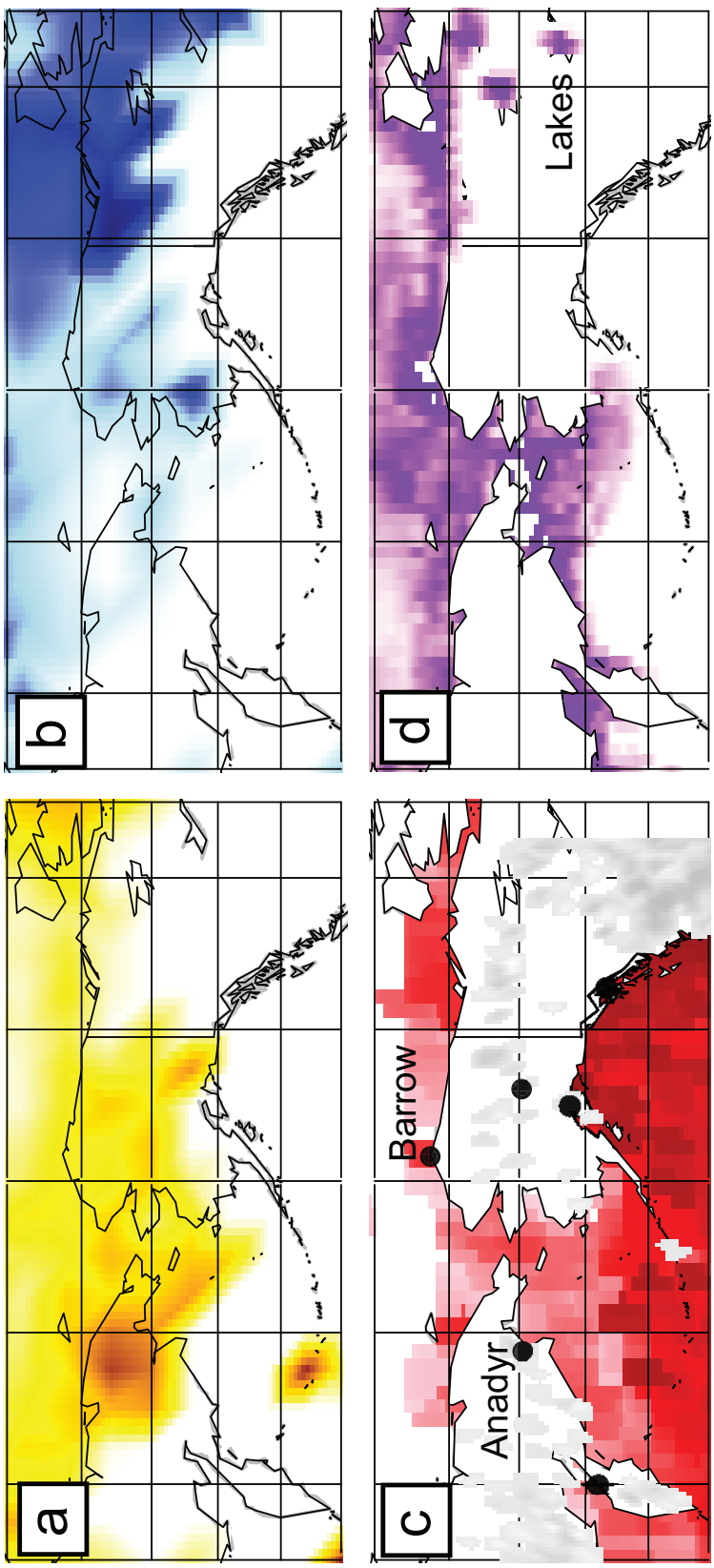

Figure 3: